Mechanisms of the negative shortwave cloud feedback in mid to high latitudes

Paulo Ceppi*, Dennis L. Hartmann,

Department of Atmospheric Sciences, University of Washington, Seattle, Washington

and Mark J. Webb

Met Office Hadley Centre, Exeter, UK

Corresponding author address: Paulo Ceppi, Department of Atmospheric Sciences, University of Washington, Box 351640, Seattle, WA 98195.

E-mail: ceppi@atmos.washington.edu

ABSTRACT

Increases in cloud optical depth and liquid water path (LWP) are robust features of global warming model simulations in high latitudes, yielding a negative shortwave cloud feedback, but the mechanisms are still uncertain. We assess the importance of microphysical processes for the negative optical depth feedback by perturbing temperature in the microphysics schemes of two aquaplanet models, both of which have separate prognostic equations for liquid water and ice. We find that most of the LWP increase with warming is caused by a suppression of ice microphysical processes in mixed-phase clouds, resulting in reduced conversion efficiencies of liquid water to ice and precipitation. Perturbing the temperature-dependent phase partitioning of convective condensate also yields a small LWP increase. Together, the perturbations in large-scale microphysics and convective condensate partitioning explain more than two-thirds of the LWP response relative to a reference case with increased SSTs, and capture all of the vertical structure of the liquid water response. We verify our findings by investigating the relationship between LWP and temperature in CMIP5 models and observations, and find very strong positive correlations between monthly-mean LWP and temperature in mixed-phase cloud regions in all models as well as in observations. We conclude that the LWP increase with warming, and the associated optical depth increase, result primarily from the temperature-dependence of ice-phase microphysical processes that deplete cloud liquid water, rather than increasing adiabatic water content as suggested in some previous studies.

1. Introduction

Despite continuning model improvement efforts, the cloud feedback remains the largest source of uncertainty in climate sensitivity estimates in global warming experiments (Soden et al. 2008; Boucher et al. 2013; Vial et al. 2013). Uncertainty in the cloud feedback is tied to the difficulty of representing complex, small-scale cloud processes in global climate models. For this reason, accurately portraying the cloud response to warming constitutes a major challenge in the development of future generations of climate models.

Most of the uncertainty in the cloud feedback is associated with the shortwave (SW) component (Soden and Vecchi 2011; Vial et al. 2013). Despite the large uncertainty, one of the few robust aspects of the SW cloud feedback predicted by climate models is a negative feedback occurring in mid to high latitudes. Unlike the positive subtropical SW cloud feedback predicted by most models, generally associated with a cloud amount decrease, the negative high-latitude feedback is mainly related to an optical thickening of the clouds, resulting in brighter and more reflective clouds (Zelinka et al. 2012; McCoy et al. 2014b; Gordon and Klein 2014).

The primary control on cloud optical depth is the vertically-integrated cloud liquid water content, or liquid water path (LWP), which has been shown to be linearly related to cloud optical depth in observations (Stephens 1978). The ice water path (IWP) also contributes to the cloud optical depth, but its effect on shortwave radiation is typically smaller due to the larger size of ice crystals compared to liquid droplets (e.g., McCoy et al. 2014a). Extratropical LWP increases have been shown to be a robust response to global warming in climate model experiments (Senior and Mitchell 1993; Colman et al. 2001; Tsushima et al. 2006; Kodama et al. 2014; Gordon and Klein 2014), and are therefore likely the main driver of the negative optical depth feedback. Understand-

ing the mechanisms of the negative SW cloud feedback in mid to high latitudes therefore requires explaining the associated LWP increases.

Various mechanisms have been proposed to explain the predicted LWP increase with warming in mid to high latitudes. On the one hand, it is natural to expect that liquid water should increase at the expense of ice in mixed-phase clouds as the climate warms (Tsushima et al. 2006; Zelinka et al. 2012; McCoy et al. 2014b; Gordon and Klein 2014). On the other hand, a LWP increase could also result from an increase in the temperature derivative of the moist adiabat with warming, causing enhanced condensation in updrafts (Betts and Harshvardhan 1987; Tselioudis et al. 1992; Gordon and Klein 2014). To further complicate the picture, changes in the hydrological cycle (Held and Soden 2006) and in atmospheric circulation (Barnes and Polvani 2013) may also impact the cloud liquid water content. The possible relevance, and relative importance, of these various processes is currently not well understood.

In this paper, we demonstrate that most of the cloud liquid water increase in mid to high latitudes in global warming experiments results from a decrease in the efficiency of the processes depleting cloud water. This is due to the suppression of ice-phase microphysical processes with warming, including not only the conversion of liquid water to ice (e.g. through the Wegener-Bergeron-Findeisen process), but also the conversion of cloud condensate to precipitation. The importance of these processes is shown by perturbing temperature in the cloud microphysics schemes of two IPCC-class climate models, which are run in aquaplanet configuration. The temperature-dependent phase partitioning of detrained condensate from convection is also shown to contribute to the global warming response, although the effect is more modest. Finally, we show that LWP is very robustly linked to temperature in mixed-phase regions in both models and observations, providing further support to the conclusions drawn from our aquaplanet model experiments. The

strong observed relationship between LWP and temperature may provide a basis to constrain the negative optical depth feedback in climate models.

We begin by presenting the changes in SW radiation, LWP, and IWP predicted by CMIP5 models in the RCP8.5 21st-century scenario in section 2. We then describe the models and the experimental setup used in this study in section 3, and present our model results in section 4. Evidence for a temperature–LWP relationship in models and observations is provided in section 5. We discuss and summarize our findings in section 6.

2. Cloud-radiative response to global warming

Shortwave cloud feedbacks in CMIP5

The multi-model mean SW cloud feedback in the RCP8.5 experiment is presented in Fig. 1a. In both hemispheres, the response features a meridional dipole, with a positive SW cloud feedback in the subtropics and lower midlatitudes ($\sim 10°$–$45°$), and a negative feedback poleward of about $50°$. The dipolar structure is reasonably robust, since more than 75% of the models agree on the sign of the feedback on either lobe of the dipole, particularly in the Southern Hemisphere. (Note that the SW cloud feedback shown in Fig. 1a includes rapid adjustments and aerosol forcing (Sherwood et al. 2015); accounting for these effects would affect the magnitude of the cloud feedback, but is unlikely to change the overall meridional structure.)

The main focus of this paper will be on the negative SW cloud feedback at mid to high latitudes, which is associated with large increases in liquid water path (LWP; Fig. 1b). The LWP increase poleward of $\sim 45°$ is a remarkably robust feature of the RCP8.5 simulations. The mean LWP response is substantial, amounting to an increase by roughly 10% per Kelvin relative to the historical multi-model mean value around $60°$. The ice water path (IWP) response is smaller, and consists

of a poleward shift of cloud ice around the midlatitudes. Because there is no compensating large decrease in IWP, total cloud water (liquid + ice) also increases in mid to high latitudes (not shown).

As discussed in the introduction, the cloud liquid water increase with warming is thought to be the main driver of the negative SW cloud feedback in high latitudes, by causing an optical thickening and brightening of the clouds (Tsushima et al. 2006; Zelinka et al. 2013; Gordon and Klein 2014; McCoy et al. 2014b). To understand the causes of the negative high-latitude feedback, it is therefore necessary to explain the mechanisms for the LWP increase.

Hypotheses for the negative extratropical cloud feedback

Several hypotheses have been proposed in the literature to explain the negative extratropical cloud feedback. We list them below and briefly discuss some open questions associated with them.

1. Phase changes in mixed-phase clouds: In mid and high latitudes, clouds are commonly mixed-phase (Warren et al. 1988) since supercooled liquid water can exist at temperatures above -38°C. Upon warming, we expect an increase in liquid water at the expense of ice in regions where mixed-phase clouds exist (Senior and Mitchell 1993; Tsushima et al. 2006; Choi et al. 2014). The transition to more liquid clouds may also yield an increase in total condensed water (liquid + ice), because liquid water droplets precipitate less efficiently than ice crystals (e.g., Senior and Mitchell 1993; Klein et al. 2009). The magnitude of the phase change effect in models and observations is still unclear, however, and is likely to depend on microphysical processes whose representation in climate models is difficult and uncertain.

2. Increases in adiabatic cloud water content: As temperature increases, the amount of water condensed in saturated updrafts also increases, assuming the rising air parcels are cooled

moist-adiabatically (Somerville and Remer 1984; Betts and Harshvardhan 1987; Tselioudis et al. 1992; Gordon and Klein 2014). It has been suggested that the cloud liquid water increases at mid to high latitudes may reflect an increase in adiabatic cloud water content with warming, which theory predicts to increase more rapidly at lower temperatures (Betts and Harshvardhan 1987; Gordon and Klein 2014). However, this argument ignores possible changes in other processes that deplete cloud liquid water, such as phase changes to ice, conversion to precipitation, or mixing of the updrafts with the environment (Tselioudis et al. 1992, 1998).

3. Poleward jet shifts: The dynamical response to global warming features a robust poleward shift of the jet streams and storm tracks, particularly in the Southern Hemisphere (Barnes and Polvani 2013). Several studies have proposed that storm track shifts may be associated with shifts in cloudiness, producing a dipole-like radiative anomaly (Bender et al. 2012; Grise et al. 2013; Boucher et al. 2013). However, more recent work has shown that the relationship between jet shifts and cloud-radiative properties is highly model-dependent (Grise and Polvani 2014; Ceppi and Hartmann 2015), and the dynamically-induced cloud response is both different in structure and much smaller in magnitude than the global warming response (Kay et al. 2014; Ceppi et al. 2014; Ceppi and Hartmann 2015), so that the poleward shift of the storm tracks is unlikely to be a dominant contribution to the negative optical depth feedback.

The aim of this paper is to test the importance of mechanism (1) for the global warming response of cloud water and the associated negative SW cloud feedback in climate models. In state-of-the-art climate models, the conversion rates between cloud liquid water, cloud ice, and precipitating particles are governed by the cloud microphysics scheme, where they are parameterized as func-

tions of temperature, moisture, and other variables. The relative amounts of cloud liquid water and ice are also influenced by the detrainment of condensate from convection, since the partitioning of detrained condensate between liquid and ice phases is often a simple function of temperature in climate models. In the next section, we present a methodology to quantify the contribution of cloud microphysics and convective condensate partitioning to the cloud water response to warming.

3. Model description and experimental setup

We run two climate models in aquaplanet configuration with prescribed sea surface temperature (SST) lower boundary conditions and perpetual equinox insolation. The models are AM2.1, developed at the Geophysical Fluid Dynamics Laboratory (The GFDL Global Atmospheric Model Development Team 2004), and the Community Earth System Model (CESM), of which we use the atmospheric component CAM5 (Hurrell et al. 2013; Neale et al. 2012). Following the aquaControl and aqua4K experiment protocol in CMIP5, we force our models with the Qobs SST profile (Neale and Hoskins 2001), and simulate the effects of global warming by applying a uniform 4 K SST increase. Because the models are symmetric about the Equator, all results presented in this paper are averages over both hemispheres. All experiments are run for a minimum of five years, after spinning up the model for a year.

To understand the cloud water response to global warming in our models, we design a set of experiments to isolate the effect of changes in cloud microphysical rates and in the phase partitioning of convective condensate with warming. As we will show, the main impact comes from the sensitivity of microphysical process rates to changes in temperature, affecting the size of the reservoirs of cloud liquid water and ice in mixed-phase regions. Below we describe the relevant model physics and the experimental design in more detail.

Cloud microphysics schemes and partitioning of convective condensate

Both models in this study include a prognostic bulk microphysics scheme with separate variables for liquid water and ice, but they use different parameterizations. We summarize the main characteristics of each scheme here, and refer the reader to the cited literature for additional detail. The cloud microphysics in AM2.1 are single-moment (predicting liquid water and ice mixing ratios only) and are mainly based on Rotstayn (1997) and Rotstayn et al. (2000). The CESM-CAM5 microphysics scheme, described in Morrison and Gettelman (2008) and Gettelman et al. (2010), predicts two moments of the particle size distribution (mixing ratios and number concentrations) for liquid water and ice separately. CESM-CAM5's microphysics are more complex than those of AM2.1, including a much larger number of processes, particularly in the ice microphysics. Note that because both cloud microphysics schemes have separate prognostic equations for liquid water and ice, the fraction of total cloud water that is in the ice phase is not a simple, explicit function of temperature. Rather, the relative amounts of liquid and ice result from the net effect of competing source and sink terms for each phase, whose rates depend on local thermodynamic conditions and other variables.

It is worth emphasizing that the cloud microphysical parameterizations apply only to the stratiform (large-scale) cloud schemes. The convection schemes use highly simplified microphysics to calculate cloud condensate mixing ratios and convective precipitation rates. In both models used in this study, the partitioning of convective condensate into liquid and ice phases is based on a simple temperature threshold. In AM2.1, detrained convective condensate is assumed to be entirely liquid at temperatures higher than -40°C. By contrast, in CESM-CAM5 the fraction of frozen condensate is a linear function of temperature, varying between 0 at -5°C and 1 at -35°C. The fraction of detrained condensate is a fixed function of the updraft detrainment level in AM2.1

(The GFDL Global Atmospheric Model Development Team 2004), while CESM-CAM5 calculates entrainment and detrainment rates between convective plumes and their environment (Neale et al. 2012).

Experimental setup

We perform a series of simulations to isolate the effects of changes in temperature on the cloud microphysical rates and on the phase partitioning of convective condensate, and quantify their impact on cloud liquid water and ice mixing ratios. The experiments are listed and described in Table 1; note that SSTs are kept at their control value in all of these experiments except SST+4K. The temperature perturbations are applied by simply increasing temperature by 4 K in the relevant sections of the code. This affects only those microphysical processes that involve the ice phase. Perturbing temperature can affect ice-phase microphysical processes in two ways. First, all processes producing (destroying) ice occur only below (above) a given temperature threshold, so increasing temperature modifies the spatial occurrence of those processes, as isotherms shift in space. Second, in CESM-CAM5 a few ice-forming process rates are explicit functions of temperature, with the rate typically increasing as temperature goes down. This includes processes such as heterogeneous and contact freezing, as well as ice multiplication via rime-splintering (Neale et al. 2012). These processes are not included in the AM2.1 microphysics.

In addition to the temperature dependence, the Wegener-Bergeron-Findeisen (WBF) mechanism (Wegener 1911; Bergeron 1935; Findeisen 1938), which converts cloud liquid water to ice or snow, also depends on the difference between saturation vapor pressure over liquid water (q_{sl}) and over ice (q_{si}), and this difference is a function of temperature. For this process only, we perturb q_{sl} and q_{si} consistent with a 4 K warming, following the Clausius-Clapeyron relationship. Other

temperature-dependent terms in the WBF process rate calculation (Rotstayn et al. 2000; Morrison and Gettelman 2008) are also adjusted for a 4 K warming.

It should be noted that the perturbed processes involve conversions between liquid water, ice, and precipitation (and subsequent melting/freezing of hydrometeors). Conversions between vapor and cloud condensate are not perturbed, with only one exception: in the CESM-CAM5 implementation, the WBF process can form cloud ice at the expense of either liquid water or vapor, depending on the availability of cloud liquid water in the grid box (Gettelman et al. 2010).

4. Results

We begin by describing the aquaplanet model responses to a 4 K SST increase (the SST+4K experiment in Table 1). The SW cloud radiative effect (CRE) and LWP responses, shown in Fig. 2a–b, look qualitatively similar to the mean RCP8.5 response in CMIP5. The aquaplanet simulations capture the negative cloud feedback in mid to high latitudes, as well as the associated LWP increase. The IWP responses are strikingly different poleward of 40° (Fig. 2c), with AM2.1 featuring an increase and CESM-CAM5 a decrease. Finally, cloud amount tends to decrease in mid–high latitudes (Fig. 2d). Cloud amount changes also explain most of the SWCRE response equatorward of 40°, consistent with the findings of Zelinka et al. (2012) for CMIP3 models. The cloud amount and IWP responses likely explain some of the differences in the SWCRE response between the models, particularly the weaker negative SW feedback in CESM-CAM5 compared to AM2.1. Despite these differences, the SWCRE response poleward of 40° appears to be dominated by the LWP increase, consistent with the stronger radiative effect of liquid droplets compared to ice crystals, which have a larger effective radius.

While we show the cloud amount response in Fig. 2 for completeness, in the remainder of this paper we will focus on the cloud liquid water and ice responses and their relationship to microphysical processes and the partitioning of convective condensate.

Cloud microphysics and partitioning of convective condensate

Figure 3 shows the LWP and IWP responses in the PCond, Micro, and Micro+PCond experiments (see Table 1), and compares them with the SST+4K response. All results in this and subsequent figures are normalized by the temperature change, assuming a 4 K warming for the Micro and PCond experiments. We begin by discussing the PCond case (red dashed curves in Fig. 3). Increasing temperature by 4 K in the partitioning of convective condensate yields a relatively small LWP increase (Fig. 3a), although the response is about twice as large in CESM-CAM5 compared to AM2.1. The smaller response in AM2.1 can be related to the choice of temperature threshold for the phase partitioning, as explained in section 3. The higher temperature threshold in CESM-CAM5 means that a larger fraction of the detrained convective condensate can be converted to ice compared to AM2.1; this results in a higher sensitivity to a temperature increase. However, part of this difference could also result from differences in the climatological amounts of convective mass flux and detrainment between the two models.

The IWP response to the PCond perturbation is also modest in both models (Fig. 3b). Somewhat counterintuitively, IWP mostly *increases* in AM2.1 around the midlatitudes; we believe this is a result of the increased cloud liquid water mixing ratio, some of which is subsequently converted to ice, rather than a direct response to the temperature perturbation. As will be shown later in this paper, in AM2.1 most of the cloud liquid water in mixed-phase clouds is converted to ice before precipitating.

The microphysical perturbations explain a much larger fraction of the LWP changes in both models (Fig. 3a, blue dotted curves). Around 50°, Micro produces about two-thirds of the SST+4K response in AM2.1, and close to half in CESM-CAM5. The LWP responses in Micro also capture the general latitude dependence of the SST+4K response remarkably well, peaking between 50° and 60°. In contrast, the IWP responses in Micro do not seem to bear much resemblance to the SST+4K response. However, we will show later in this section that key aspects of the vertical structure of the cloud ice response are indeed reproduced by the Micro experiments.

Applying the Micro and PCond forcings together (thick grey curves in Fig. 3) yields LWP changes that are even closer to the SST+4K response, generally explaining more than two-thirds of the response around the midlatitudes. For both LWP and IWP, the Micro and PCond perturbations are nearly additive. The resemblance between the Micro+PCond and SST+4K cloud liquid water responses is even more striking when considering the vertical structure of the cloud water mixing ratio changes (Fig. 4). In both models, most of the response occurs in a band upward and poleward of the freezing line (black curves in Fig. 4). The liquid water increase also occurs just upward and poleward of the climatological distribution (grey contours in Fig. 4), resulting in a net increase and poleward expansion of the climatological LWP. The vertical structure and general temperature dependence of the cloud liquid water response to warming is very consistent with the results of Senior and Mitchell (1993), Tsushima et al. (2006), and Choi et al. (2014), all of whom also noted the coupling between the freezing isotherm and the cloud liquid water response. This coupling suggests an important control of temperature on microphysical process rates and the cloud liquid water reservoir, which we will further explore in the next section.

The vertical cross-sections of the cloud ice mixing ratio response (Fig. 5) also show that the Micro+PCond experiment does capture a significant part of the cloud ice response to warming. In AM2.1, there is a large cloud ice decrease right above the freezing line, where ice is forced to

melt upon warming. However, the SST+4K experiment features an additional increase in cloud ice at higher altitudes that is mostly absent from Micro+PCond, explaining the discrepancy between the vertically-integrated responses shown in Fig. 3. In CESM-CAM5, there is no large ice response near the freezing line, consistent with the climatological cloud ice distribution being centered further poleward and away from the freezing isotherm compared to AM2.1 (grey contours in Fig. 5). It is also interesting to note that the cloud ice mixing ratio is generally much smaller in CESM-CAM5. While the Micro+PCond experiment does produce a decrease in cloud ice, it underestimates the response compared to SST+4K. CESM-CAM5 has a temperature-dependent activation for ice nuclei in the aerosol scheme, which we have not perturbed in the experiments presented here. However, we have verified in separate experiments that the aerosol activation does not contribute significantly to the cloud ice response to warming (not shown).

Taken together, the results presented in this section show that the cloud liquid water content of mixed-phase clouds is strongly controlled by the temperature dependence of microphysical process rates, and to a lesser degree by the temperature dependence of the partitioning of convective condensate. This suggests that a large fraction of the global warming response of cloud liquid water can be attributed to the direct effect of warming, rather than other processes such as adiabatic increases in moisture content with warming, changes in moisture convergence, or changes in radiative heating rates, at least in the two models considered in this study. While important aspects of the cloud ice response are also explained by the microphysics and convective condensate partitioning perturbations, additional processes would need to be considered to capture the full global warming response of cloud ice in our two models. In the next section, we study the microphysical processes in more detail and explain how their temperature dependence controls the cloud liquid water content.

Microphysical processes

As discussed in section 3, the cloud microphysics schemes in AM2.1 and CESM-CAM5 are prognostic, so that the scheme calculates conversion rates between water vapor, cloud liquid water, cloud ice, and precipitation, based on physical parameterizations of the relevant processes. Thus, the liquid water and ice content of clouds is ultimately determined by the relative efficiency of their respective sources and sinks. From this perspective, the response of cloud liquid water and ice to warming can be thought of as resulting from changes in the relative efficiencies of the corresponding source and sink terms.

The microphysical conversions are depicted schematically in Fig. 6, using the rates output directly by the model. The arrows in Fig. 6 point in the direction of the net vertically-integrated conversion rate at 50°, with the arrow thickness proportional to the conversion rate. (Note that the fluxes between vapor and condensate are dominated by large-scale condensation from the cloud *macrophysics* scheme, as well as detrainment of condensate from convection, rather than by microphysical processes.) The schematic shows that in both models, there is a net source of cloud liquid water from condensation, and net sinks from conversion of liquid water to ice and precipitation. However, the relative importance of the liquid water sinks differs greatly between the models: while in AM2.1 almost all of the liquid water is converted to ice before precipitating, in CESM-CAM5 most of the liquid water is directly converted to precipitation, with little net conversion to ice. The varying importance of the sources and sinks of cloud liquid water and ice suggest that the microphysical processes responsible for the cloud water response to warming may be different in the two models.

Part of the inter-model differences in Fig. 6 reflect different philosophies in the implementation of certain microphysical processes. For example, growth of ice crystals through the WBF process

is saved as a flux from liquid to ice in AM2.1, while in CESM-CAM5 is it may be saved as liquid to ice or vapor to ice, depending on the availability of liquid water in the grid box (see Gettelman et al. 2010); however, in reality this is a multi-step process involving condensation, reevaporation, and deposition onto ice, but these multiple steps are represented in neither of the schemes. Thus, differences in the fluxes in Fig. 6 partly result from somewhat arbitrary choices in the representation of the microphysics.

To gain additional insight into the mechanisms of the microphysical response to warming, we group the microphysical processes into two categories, and perturb temperature in each of them separately. We consider processes involved in the conversion between liquid water and ice ($\text{Micro}_{\text{L}\leftrightarrow\text{I}}$), and all precipitation processes (Micro_{P}). The latter category includes the conversion of cloud condensate to precipitation, as well as the subsequent freezing or melting of hydrometeors. The two experiments are described in Table 1.

Figure 7 shows the separate contributions of $\text{Micro}_{\text{L}\leftrightarrow\text{I}}$ and Micro_{P} to the LWP response to warming. In AM2.1, the largest contribution to the LWP increase is from the conversion between liquid water and ice (green dashed curves in Fig. 7), consistent with this conversion mechanism being the largest sink of cloud liquid water. Upon warming, the conversion efficiency of liquid water to ice is reduced, leading to an increase of the liquid water reservoir until the net conversion rate of liquid water to ice is sufficiently large to balance the source terms. The same perturbation leaves the IWP nearly unchanged (Fig. 7b, left), likely because the increase in cloud liquid water balances the decreased conversion efficiency of liquid water to ice.

The second largest impact on the LWP response in AM2.1 comes from the precipitation processes, which also cause all of the IWP decrease seen in the Micro experiment (orange dotted curves in Fig. 7). The IWP decrease results from the fact that in the AM2.1 cloud microphysics, all melting cloud ice is assumed to convert to rain rather than cloud liquid water, so ice melting is

regarded as a precipitation process here. The temperature increase thus forces the melting of ice in regions near the freezing line. We interpret the associated LWP increase in AM2.1 as an indirect result of the IWP decrease, since none of the precipitation processes involving cloud liquid water are temperature-dependent (in contrast to CESM-CAM5, as explained below). With less ice available, the conversion rate from liquid water to ice (mainly through the WBF process and through riming, see Table 1) decreases, allowing the cloud liquid water content to increase.

By contrast, in CESM-CAM5 almost all of the microphysical LWP and IWP response originates from the precipitation processes alone. The small $\text{Micro}_{\text{L}\leftrightarrow\text{I}}$ response is consistent with the small net conversion rate between liquid water and ice in CESM-CAM5 (cf. Fig. 6). The LWP increase in Micro_{P} implies a general decrease in the conversion efficiency of cloud liquid water to precipitation. While conversion rates of liquid water to rain are not temperature-sensitive, the CESM-CAM5 microphysics includes several temperature-dependent processes converting liquid water to snow. Thus, the results suggest that the suppression of the precipitation conversion from liquid water to snow may be responsible for much of the LWP increase in the Micro experiment in CESM-CAM5. The small IWP response in CAM5 is also mainly associated with the precipitation processes; the weak IWP increase between 50° and 70° appears to be caused by a decreased efficiency of precipitation formation from cloud ice.

In general, the sum of the $\text{Micro}_{\text{L}\leftrightarrow\text{I}}$ and Micro_{P} perturbations is close to the Micro response for both models, indicating that the perturbations are approximately linearly additive (grey and black curves in Fig. 7).

In summary, the main finding of this section is that cloud liquid water increases result mainly from the suppression of ice microphysical processes upon warming, which deplete liquid water by converting it to ice or precipitation. The resulting increase in condensed water with warming is consistent with the notion that clouds containing ice precipitate more efficiently (Senior and

Mitchell 1993; Tsushima et al. 2006; Gordon and Klein 2014; Komurcu et al. 2014). This suggests that an accurate parameterization of ice growth and precipitation processes is crucial for the representation of the climatology and forced response of cloud water content in climate models.

5. Temperature–LWP relationship in CMIP5 models and observations

We have shown that the temperature dependence of microphysical process rates and of the phase partitioning of convective condensate explains most of the cloud liquid water increase in mid and high latitudes in two climate models, AM2.1 and CESM-CAM5. In this section, we present evidence supporting this conclusion in other climate models and observations. One key aspect of our results is that temperature alone controls most of the LWP changes in mixed-phase clouds. If this is generally the case in models and observations, then the following two hypotheses can be made:

1. There is a robust positive relationship between temperature and cloud liquid water in mid to high latitudes.

2. The cloud liquid water response to unforced (e.g., seasonal) temperature variations is similar to the forced response.

We test our two hypotheses by calculating correlation and regression coefficients for monthly-mean temperature–LWP relationships in models and observations. The data include output from 32 CMIP5 models, as well as satellite LWP retrievals for 1989–2008 (O'Dell et al. 2008) combined with reanalysis temperature from ERA-Interim (Dee et al. 2011). For simplicity, we use temperature at 850 hPa, the level closest to the peak cloud liquid water mixing ratio in most models (not shown), and average the data zonally before calculating the correlations and regressions. Because satellite LWP observations are only available over the oceans, we remove land grid points

from the model data to ensure that the results are comparable between models and observations, but note that the model results are very similar if land areas are included (not shown).

In agreement with hypothesis (1), models and observations feature strong positive correlations between temperature and LWP in mid- and high-latitude regions in both hemispheres (Fig. 8a). The correlations are particularly high in the observations, peaking at 0.95 near 50°. The latitude beyond which the correlations become positive varies considerably among models, and may reflect differences in the meridional extent of mixed-phase regions. It should also be noted that the observations feature positive LWP–temperature correlations at lower latitudes than the majority of the models. Over the Southern Ocean poleward of 60° S, the LWP–temperature correlation becomes lower in observations than in models; it is unclear whether this reflects a different LWP–temperature relationship in the observations, or whether it is related to measurement errors, for example over sea ice regions.

Consistent with the positive correlation coefficients, all models (as well as the observations) produce a LWP increase around the midlatitudes for increasing 850 hPa temperature, although there is substantial inter-model variability in the magnitude and meridional structure of the LWP regression coefficients (Fig. 8b). The strong positive LWP–temperature relationships are consistent with the results of Gordon and Klein (2014), who found positive condensed water path–temperature relationships in models and observations for low clouds with cloud-top temperatures below freezing. Earlier studies based on in-situ observations also found similar relationships in cold clouds (Feigelson 1978; Gultepe and Isaac 1997). We believe that regions of positive regression and correlation coefficients correspond to regions where clouds are predominantly mixed-phase, and where LWP is therefore mainly controlled by temperature-dependent ice-phase microphysical processes.

Comparing models with observations, we note that models are in general agreement with the observed LWP–temperature relationship, especially in the Northern Hemisphere (Fig. 8b). How-

ever, many models largely overestimate the LWP increase with warming between 50° and 70° S; this may result from most models overestimating the glaciation temperature, which is linked to a larger LWP response to warming (McCoy et al., manuscript submitted to J. Geophys. Res.). Despite these differences, the key result is that the observed LWP–temperature relationships support the idea of a negative SW cloud feedback in mid to high latitudes, driven by increases in cloud liquid water content. We further discuss this idea below.

The LWP response in RCP8.5 (normalized by the local warming in each model) looks remarkably similar to the regression coefficients (compare panels (b) and (c) in Fig. 8), both in terms of magnitude and meridional structure of the response. The relative order of the models is also similar, so that models with very positive regression coefficients tend to produce a very large LWP increase with global warming, and vice-versa. Gordon and Klein (2014) found a similar time-scale invariance in the relationship between total cloud water content and temperature in a smaller set of climate models. This result provides hope that it may be possible to constrain the SW cloud feedback in mid to high latitudes using observed LWP–temperature relationships. The results in Fig. 8b also suggest that the negative SW cloud feedback predicted by models may be too negative over the Southern Ocean. We will explore these ideas in future work.

We repeated the analysis shown in Fig. 8 for IWP (not shown). The IWP–temperature correlations are generally negative, and strongest near 40°. However, we found that the IWP–temperature regression coefficients bore less similarity to the IWP changes in RCP8.5, consistent with our result that the temperature increase does not control all aspects of the forced cloud ice response. Models tend to disagree on the sign of the IWP response in RCP8.5, but the multi-model mean response is a weak decrease equatorward of 50°, and a weak increase poleward thereof (cf. Fig. 1c).

6. Summary and conclusions

A robust feature of global warming model experiments is a negative shortwave cloud feedback in mid to high latitudes, driven by an optical thickening of the clouds associated with liquid water path (LWP) increases. We investigate the processes involved in the LWP response by perturbing temperature in the cloud microphysics schemes of two climate models in aquaplanet configuration, GFDL AM2.1 and CESM-CAM5, both of which have separate prognostic equations for liquid water and ice. We demonstrate that most of the LWP increase is a direct response to warming through a decrease in the efficiency of liquid water sinks, resulting in a larger reservoir of cloud liquid water. This occurs because temperature-dependent ice-phase microphysical processes are suppressed upon warming, reducing the efficiency of precipitation and conversion to ice, the two microphysical sinks for liquid water. An additional smaller contribution to the LWP increase comes from the phase partitioning of detrained convective condensate, which is based on a simple temperature threshold in both models. Taken together, the microphysics and the partitioning of convective condensate explain about two-thirds of the LWP response to increasing SST in CESM-CAM5, and an even higher fraction in AM2.1.

While important aspects of the cloud ice response to warming are also reproduced in our experiments with perturbed microphysics, changes in ice water path (IWP) with increasing SST are not quantitatively predicted by increasing temperature in the cloud microphysics alone. Our two models also disagree on the IWP response to SST increase. This result is consistent with the IWP response being much less robust than the LWP response in RCP8.5 simulations of CMIP5 models. However, the larger radiative impact of small liquid droplets (compared to relatively large ice crystals) means that the shortwave cloud feedback is primarily determined by the LWP response.

In support of the conclusion drawn from our model experiments, we show that a strong positive relationship between temperature and LWP exists in both models and observations. This positive relationship occurs only in mid and high latitudes, where mixed-phase clouds are expected to occur. Interestingly, the model-specific temperature–LWP relationships from monthly variability are reflected in the different LWP responses to global warming, so the temperature dependence of LWP in mixed-phase regions appears to be largely time-scale invariant. This provides hope that observed relationships can provide a constraint on future LWP increases and on the associated shortwave cloud feedback.

Our results indicate that a fraction of the LWP response cannot be ascribed to a decrease in the efficiency of cloud liquid water sinks with warming. This is unsurprising, since it is to be expected that the liquid water *sources* might also respond to warming. Processes likely to also contribute to the LWP increase include

1. the increase in the temperature derivative of the moist adiabat, causing the adiabatic cloud water content to go up in saturated updrafts; and

2. the general increase in radiative cooling as the atmosphere becomes more emissive with warming, which must be balanced by enhanced latent heating and precipitation, at least on global scales.

Both of these effects would be expected to yield an enhanced rate of formation of cloud water as the atmosphere warms. Based on our results, however, changes in the liquid water sink terms exert a stronger control on the LWP response to warming. While atmospheric circulation changes could also affect cloud water content, a regression analysis of LWP and IWP on zonal-mean jet latitude indicated that this is unlikely to be a major effect in our two models (not shown), as the cloud water changes associated with jet variability are small. This appears consistent with previous work

showing the much larger impact of thermodynamic effects on cloud-radiative properties compared to dynamical effects (Ceppi and Hartmann 2015).

Our results suggest two important directions for future research. First, improved global-scale observations of cloud properties are needed to develop observational constraints on climate model behavior. For example, large uncertainties in cloud ice observations exist (e.g., Heymsfield et al. 2008), making an accurate estimation of model biases difficult. Second, an improved representation of ice-phase microphysical processes appears to be crucial to reduce the large model errors in both the present-day climatology and future response of condensed cloud water (Choi et al. 2014; Komurcu et al. 2014). In-situ measurements and laboratory experiments will likely be necessary to constrain the model climatologies and improve current parameterization schemes. Progress on those issues will ultimately contribute to reducing the uncertainty in the cloud feedback, and will alleviate pervasive climatological biases associated with midlatitude clouds (Hwang and Frierson 2013; Ceppi et al. 2012).

Acknowledgments. We are grateful to Chris Bretherton, Andrew Gettelman, and Rob Wood for very helpful discussions and comments. P. Ceppi and D. L. Hartmann were supported by the National Science Foundation under grant AGS-0960497. M. Webb was supported by the Joint DECC / Defra Met Office Hadley Centre Climate Programme (GA01101).

References

Barnes, E. A., and L. Polvani, 2013: Response of the midlatitude jets and of their variability to increased greenhouse gases in the CMIP5 models. *Journal of Climate*, **26 (18)**, 7117–7135, doi:10.1175/JCLI-D-12-00536.1, URL http://journals.ametsoc.org/doi/abs/10.1175/JCLI-D-12-00536.1.

Bender, F. A.-M., V. Ramanathan, and G. Tselioudis, 2012: Changes in extratropical storm track cloudiness 19832008: observational support for a poleward shift. *Climate Dynamics*, **38 (9-10)**, 2037–2053, doi:10.1007/s00382-011-1065-6, URL http://link.springer.com/10.1007/s00382-011-1065-6.

Bergeron, T., 1935: On the physics of clouds and precipitation. *Procès-Verbaux de l'Association de Météorologie*, International Union of Geodesy and Geophysics, Paris, France, 156–178.

Betts, A. K., and Harshvardhan, 1987: Thermodynamic constraint on the cloud liquid water feedback in climate models. *Journal of Geophysical Research*, **92 (D7)**, 8483, doi:10.1029/JD092iD07p08483, URL http://doi.wiley.com/10.1029/JD092iD07p08483.

Boucher, O., and Coauthors, 2013: Clouds and Aerosols. *Climate Change 2013: The Physical Science Basis. Contribution of Working Group I to the Fifth Assessment Report of the Intergovernmental Panel on Climate Change*, T. F. Stocker, D. Qin, P. G.-K, M. Tignor, S. K. Allen, J. Boschung, A. Nauels, Y. Xia, V. Bex, and P. M. Midgley, Eds., Cambridge University Press, Cambridge, United Kingdom and New York, NY, USA, 571–657.

Ceppi, P., and D. L. Hartmann, 2015: Connections Between Clouds, Radiation, and Midlatitude Dynamics: a Review. *Current Climate Change Reports*, **1 (2)**, 94–102, doi:10.1007/s40641-015-0010-x, URL http://link.springer.com/10.1007/s40641-015-0010-x.

Ceppi, P., Y.-T. Hwang, D. M. W. Frierson, and D. L. Hartmann, 2012: Southern Hemisphere jet latitude biases in CMIP5 models linked to shortwave cloud forcing. *Geophysical Research Letters*, **39 (19)**, L19 708, doi:10.1029/2012GL053115, URL http://www.agu.org/pubs/crossref/2012/2012GL053115.shtml.

528 Ceppi, P., M. D. Zelinka, and D. L. Hartmann, 2014: The response of the Southern Hemispheric
529 eddy-driven jet to future changes in shortwave radiation in CMIP5. *Geophysical Research*
530 *Letters*, **41 (9)**, 3244–3250, doi:10.1002/2014GL060043, URL http://doi.wiley.com/10.1002/
531 2014GL060043.

532 Choi, Y.-S., C.-H. Ho, C.-E. Park, T. Storelvmo, and I. Tan, 2014: Influence of cloud phase
533 composition on climate feedbacks. *Journal of Geophysical Research: Atmospheres*, **119 (7)**,
534 3687–3700, doi:10.1002/2013JD020582, URL http://doi.wiley.com/10.1002/2013JD020582.

535 Colman, R., J. Fraser, and L. Rotstayn, 2001: Climate feedbacks in a general circulation
536 model incorporating prognostic clouds. *Climate Dynamics*, **18 (1-2)**, 103–122, doi:10.1007/
537 s003820100162, URL http://link.springer.com/10.1007/s003820100162.

538 Dee, D. P., and Coauthors, 2011: The ERA-Interim reanalysis: configuration and performance of
539 the data assimilation system. *Quarterly Journal of the Royal Meteorological Society*, **137 (656)**,
540 553–597, doi:10.1002/qj.828, URL http://doi.wiley.com/10.1002/qj.828.

541 Feigelson, E. M., 1978: Preliminary radiation model of a cloudy atmosphere. Part I: Structure of
542 clouds and solar radiation. *Beiträge zur Physik der Atmosphäre*, **51**, 203–229.

543 Findeisen, W., 1938: Die kolloidmeteorologischen Vorgänge bei Niederschlagsbildung. *Meteorol-*
544 *ogische Zeitschrift*, **55**, 121–133.

545 Gettelman, A., and Coauthors, 2010: Global simulations of ice nucleation and ice supersaturation
546 with an improved cloud scheme in the Community Atmosphere Model. *Journal of Geophysi-*
547 *cal Research*, **115 (D18)**, D18 216, doi:10.1029/2009JD013797, URL http://doi.wiley.com/10.
548 1029/2009JD013797.

549 Gordon, N. D., and S. A. Klein, 2014: Low-cloud optical depth feedback in climate models. *Jour-*
550 *nal of Geophysical Research: Atmospheres*, **119 (10)**, 6052–6065, doi:10.1002/2013JD021052,
551 URL http://doi.wiley.com/10.1002/2013JD021052.

552 Grise, K. M., and L. M. Polvani, 2014: Southern Hemisphere Cloud-Dynamics Biases
553 in CMIP5 Models and Their Implications for Climate Projections. *Journal of Climate*,
554 **27 (15)**, 6074–6092, doi:10.1175/JCLI-D-14-00113.1, URL http://journals.ametsoc.org/doi/
555 abs/10.1175/JCLI-D-14-00113.1.

556 Grise, K. M., L. M. Polvani, G. Tselioudis, Y. Wu, and M. D. Zelinka, 2013: The ozone hole
557 indirect effect: Cloud-radiative anomalies accompanying the poleward shift of the eddy-driven
558 jet in the Southern Hemisphere. *Geophysical Research Letters*, **40 (14)**, 3688–3692, doi:10.
559 1002/grl.50675, URL http://doi.wiley.com/10.1002/grl.50675.

560 Gultepe, I., and G. A. Isaac, 1997: Liquid Water Content and Temperature Relationship from
561 Aircraft Observations and Its Applicability to GCMs. *Journal of Climate*, **10 (3)**, 446–452, doi:
562 10.1175/1520-0442(1997)010⟨0446:LWCATR⟩2.0.CO;2, URL http://journals.ametsoc.org/doi/
563 abs/10.1175/1520-0442\%281997\%29010\%3C0446\%3ALWCATR\%3E2.0.CO\%3B2.

564 Held, I. M., and B. J. Soden, 2006: Robust Responses of the Hydrological Cycle to Global Warm-
565 ing. *Journal of Climate*, **19 (21)**, 5686–5699, doi:10.1175/JCLI3990.1, URL http://journals.
566 ametsoc.org/doi/abs/10.1175/JCLI3990.1.

567 Heymsfield, A. J., and Coauthors, 2008: Testing IWC Retrieval Methods Using Radar and Ancil-
568 lary Measurements with In Situ Data. *Journal of Applied Meteorology and Climatology*, **47 (1)**,
569 135–163, URL http://journals.ametsoc.org/doi/abs/10.1175/2007JAMC1606.1.

570 Hurrell, J. W., and Coauthors, 2013: The Community Earth System Model: A Framework
571 for Collaborative Research. *Bulletin of the American Meteorological Society*, **94 (9)**, 1339–
572 1360, doi:10.1175/BAMS-D-12-00121.1, URL http://journals.ametsoc.org/doi/abs/10.1175/
573 BAMS-D-12-00121.1.

574 Hwang, Y.-T., and D. M. W. Frierson, 2013: Link between the double-Intertropical Convergence
575 Zone problem and cloud biases over the Southern Ocean. *Proceedings of the National Academy*
576 *of Sciences of the United States of America*, **110 (13)**, 4935–40, doi:10.1073/pnas.1213302110,
577 URL http://www.pnas.org/content/110/13/4935.

578 Kay, J. E., B. Medeiros, Y.-T. Hwang, A. Gettelman, J. Perket, and M. G. Flanner, 2014: Pro-
579 cesses controlling Southern Ocean Shortwave Climate Feedbacks in CESM. *Geophysical Re-*
580 *search Letters*, **41**, 616–622, doi:10.1002/2013GL058315, URL http://doi.wiley.com/10.1002/
581 2013GL058315.

582 Klein, S. A., and Coauthors, 2009: Intercomparison of model simulations of mixed-phase clouds
583 observed during the ARM Mixed-Phase Arctic Cloud Experiment. I: single-layer cloud. *Quar-*
584 *terly Journal of the Royal Meteorological Society*, **135 (641)**, 979–1002, doi:10.1002/qj.416,
585 URL http://doi.wiley.com/10.1002/qj.416.

586 Kodama, C., S. Iga, and M. Satoh, 2014: Impact of the sea surface temperature rise on storm-track
587 clouds in global nonhydrostatic aqua planet simulations. *Geophysical Research Letters*, **41 (10)**,
588 3545–3552, doi:10.1002/2014GL059972, URL http://doi.wiley.com/10.1002/2014GL059972.

589 Komurcu, M., and Coauthors, 2014: Intercomparison of the cloud water phase among global
590 climate models. *Journal of Geophysical Research: Atmospheres*, **119 (6)**, 3372–3400, doi:10.
591 1002/2013JD021119, URL http://doi.wiley.com/10.1002/2013JD021119.

McCoy, D. T., D. L. Hartmann, and D. P. Grosvenor, 2014a: Observed Southern Ocean Cloud Properties and Shortwave Reflection. Part I: Calculation of SW Flux from Observed Cloud Properties. *Journal of Climate*, 141014122513007, doi:10.1175/JCLI-D-14-00287.1, URL http://journals.ametsoc.org/doi/abs/10.1175/JCLI-D-14-00287.1.

McCoy, D. T., D. L. Hartmann, and D. P. Grosvenor, 2014b: Observed Southern Ocean Cloud Properties and Shortwave Reflection. Part II: Phase changes and low cloud feedback. *Journal of Climate*, 141006071055006, doi:10.1175/JCLI-D-14-00288.1, URL http://journals.ametsoc.org/doi/abs/10.1175/JCLI-D-14-00288.1.

Morrison, H., and A. Gettelman, 2008: A New Two-Moment Bulk Stratiform Cloud Microphysics Scheme in the Community Atmosphere Model, Version 3 (CAM3). Part I: Description and Numerical Tests. *Journal of Climate*, **21 (15)**, 3642–3659, doi:10.1175/2008JCLI2105.1, URL http://journals.ametsoc.org/doi/abs/10.1175/2008JCLI2105.1.

Neale, R. B., and Coauthors, 2012: Description of the NCAR Community Atmosphere Model (CAM 5.0). *NCAR Tech. Note TN-486*, 274.

O'Dell, C. W., F. J. Wentz, and R. Bennartz, 2008: Cloud Liquid Water Path from Satellite-Based Passive Microwave Observations: A New Climatology over the Global Oceans. *Journal of Climate*, **21 (8)**, 1721–1739, doi:10.1175/2007JCLI1958.1, URL http://journals.ametsoc.org/doi/abs/10.1175/2007JCLI1958.1.

Rotstayn, L. D., 1997: A physically based scheme for the treatment of stratiform clouds and precipitation in large-scale models. I: Description and evaluation of the microphysical processes. *Quarterly Journal of the Royal Meteorological Society*, **123 (541)**, 1227–1282, doi:10.1002/qj.49712354106, URL http://doi.wiley.com/10.1002/qj.49712354106.

Rotstayn, L. D., B. F. Ryan, and J. J. Katzfey, 2000: A Scheme for Calculation of the Liquid Fraction in Mixed-Phase Stratiform Clouds in Large-Scale Models. *Monthly Weather Review*, **128 (4)**, 1070–1088, doi:10.1175/1520-0493(2000)128⟨1070:ASFCOT⟩2.0.CO;2, URL http://journals.ametsoc.org/doi/abs/10.1175/1520-0493(2000)128⟨1070:ASFCOT⟩2.0.CO;2.

Senior, C. A., and J. F. B. Mitchell, 1993: Carbon Dioxide and Climate. The Impact of Cloud Parameterization. *Journal of Climate*, **6 (3)**, 393–418, doi:10.1175/1520-0442(1993)006⟨0393:CDACTI⟩2.0.CO;2, URL http://journals.ametsoc.org/doi/abs/10.1175/1520-0442\%281993\%29006\%3C0393\%3ACDACTI\%3E2.0.CO\%3B2.

Sherwood, S. C., S. Bony, O. Boucher, C. Bretherton, P. M. Forster, J. M. Gregory, and B. Stevens, 2015: Adjustments in the Forcing-Feedback Framework for Understanding Climate Change. *Bulletin of the American Meteorological Society*, **96 (2)**, 217–228, doi:10.1175/BAMS-D-13-00167.1, URL http://journals.ametsoc.org/doi/abs/10.1175/BAMS-D-13-00167.1.

Soden, B. J., I. M. Held, R. Colman, K. M. Shell, J. T. Kiehl, and C. A. Shields, 2008: Quantifying Climate Feedbacks Using Radiative Kernels. *Journal of Climate*, **21 (14)**, 3504–3520, doi:10.1175/2007JCLI2110.1, URL http://journals.ametsoc.org/doi/abs/10.1175/2007JCLI2110.1.

Soden, B. J., and G. A. Vecchi, 2011: The vertical distribution of cloud feedback in coupled ocean-atmosphere models. *Geophysical Research Letters*, **38 (12)**, L12 704, doi:10.1029/2011GL047632, URL http://doi.wiley.com/10.1029/2011GL047632.

Somerville, R. C. J., and L. A. Remer, 1984: Cloud optical thickness feedbacks in the CO2 climate problem. *Journal of Geophysical Research*, **89 (D6)**, 9668, doi:10.1029/JD089iD06p09668, URL http://doi.wiley.com/10.1029/JD089iD06p09668.

Stephens, G. L., 1978: Radiation Profiles in Extended Water Clouds. II: Parameterization Schemes. *Journal of the Atmospheric Sciences*, **35 (11)**, 2123–2132, doi:10.1175/1520-0469(1978)035⟨2123:RPIEWC⟩2.0.CO;2, URL http://journals.ametsoc.org/doi/abs/10.1175/1520-0469(1978)035\%3C2123\%3ARPIEWC\%3E2.0.CO\%3B2.

Taylor, K. E., M. Crucifix, P. Braconnot, C. D. Hewitt, C. Doutriaux, A. J. Broccoli, J. F. B. Mitchell, and M. J. Webb, 2007: Estimating Shortwave Radiative Forcing and Response in Climate Models. *Journal of Climate*, **20 (11)**, 2530–2543, doi:10.1175/JCLI4143.1, URL http://journals.ametsoc.org/doi/abs/10.1175/JCLI4143.1.

The GFDL Global Atmospheric Model Development Team, 2004: The New GFDL Global Atmosphere and Land Model AM2LM2: Evaluation with Prescribed SST Simulations. *Journal of Climate*, **17 (24)**, 4641–4673, doi:10.1175/JCLI-3223.1, URL http://journals.ametsoc.org/doi/abs/10.1175/jcli-3223.1.

Tselioudis, G., A. D. DelGenio, W. Kovari, and M.-S. Yao, 1998: Temperature Dependence of Low Cloud Optical Thickness in the GISS GCM: Contributing Mechanisms and Climate Implications. *Journal of Climate*, **11 (12)**, 3268–3281, doi:10.1175/1520-0442(1998)011⟨3268:TDOLCO⟩2.0.CO;2, URL http://journals.ametsoc.org/doi/abs/10.1175/1520-0442(1998)011\%3C3268:TDOLCO\%3E2.0.CO\%3B2.

Tselioudis, G., W. B. Rossow, and D. Rind, 1992: Global Patterns of Cloud Optical Thickness Variation with Temperature. *Journal of Climate*, **5 (12)**, 1484–1495, doi:10.1175/1520-0442(1992)005⟨1484:GPOCOT⟩2.0.CO;2, URL http://journals.ametsoc.org/doi/abs/10.1175/1520-0442(1992)005⟨1484:GPOCOT⟩2.0.CO;2.

Tsushima, Y., and Coauthors, 2006: Importance of the mixed-phase cloud distribution in the control climate for assessing the response of clouds to carbon dioxide increase: a multi-

model study. *Climate Dynamics*, **27 (2-3)**, 113–126, doi:10.1007/s00382-006-0127-7, URL http://link.springer.com/10.1007/s00382-006-0127-7.

Vial, J., J.-L. Dufresne, and S. Bony, 2013: On the interpretation of inter-model spread in CMIP5 climate sensitivity estimates. *Climate Dynamics*, **41 (11-12)**, 3339–3362, doi:10.1007/s00382-013-1725-9, URL http://link.springer.com/10.1007/s00382-013-1725-9.

Warren, S., C. Hahn, J. London, R. Chervin, and R. Jenne, 1988: Global Distribution of Total Cloud Cover and Cloud Type Amounts Over the Ocean. Tech. rep. URL http://opensky.library.ucar.edu/collections/TECH-NOTE-000-000-000-467.

Wegener, A., 1911: *Thermodynamik der Atmosphäre*. Leipzig, Germany, 331 pp.

Zelinka, M. D., S. A. Klein, and D. L. Hartmann, 2012: Computing and Partitioning Cloud Feedbacks Using Cloud Property Histograms. Part II: Attribution to Changes in Cloud Amount, Altitude, and Optical Depth. *Journal of Climate*, **25 (11)**, 3736–3754, doi:10.1175/JCLI-D-11-00249.1, URL http://journals.ametsoc.org/doi/abs/10.1175/JCLI-D-11-00249.1.

Zelinka, M. D., S. A. Klein, K. E. Taylor, T. Andrews, M. J. Webb, J. M. Gregory, and P. M. Forster, 2013: Contributions of Different Cloud Types to Feedbacks and Rapid Adjustments in CMIP5. *Journal of Climate*, **26 (14)**, 5007–5027, doi:10.1175/JCLI-D-12-00555.1, URL http://journals.ametsoc.org/doi/abs/10.1175/JCLI-D-12-00555.1.

LIST OF TABLES

TABLE 1. List of experiments described in this paper. The following symbols are used: PCond for the partitioning of convective condensate, Micro for microphysics, L for liquid water, I for ice, P for precipitation. The list of processes involved in each experiment depends on the details of the microphysics scheme.

Experiment name	Description	Typical processes involved
$\text{Micro}_{\text{L}\leftrightarrow\text{I}}$	perturb temperature-dependent microphysical processes involving conversion between liquid water and ice	melting, homogeneous/heterogeneous freezing, riming, Wegener-Bergeron-Findeisen
Micro_{P}	perturb temperature-dependent microphysical processes involving precipitation	accretion, autoconversion, Wegener-Bergeron-Findeisen (liquid water to snow)
Micro	perturb all temperature-dependent microphysical processes	all of the above plus homogeneous/heterogeneous ice nucleation and adjustment (removal of excess supersaturation)
PCond	perturb temperature threshold for partitioning of detrained convective condensate	detrainment of convective condensate to the grid-scale environment
Micro+PCond	Micro and PCond perturbations together	all processes in Micro and PCond
SST+4K	uniform 4 K SST increase	-

LIST OF FIGURES

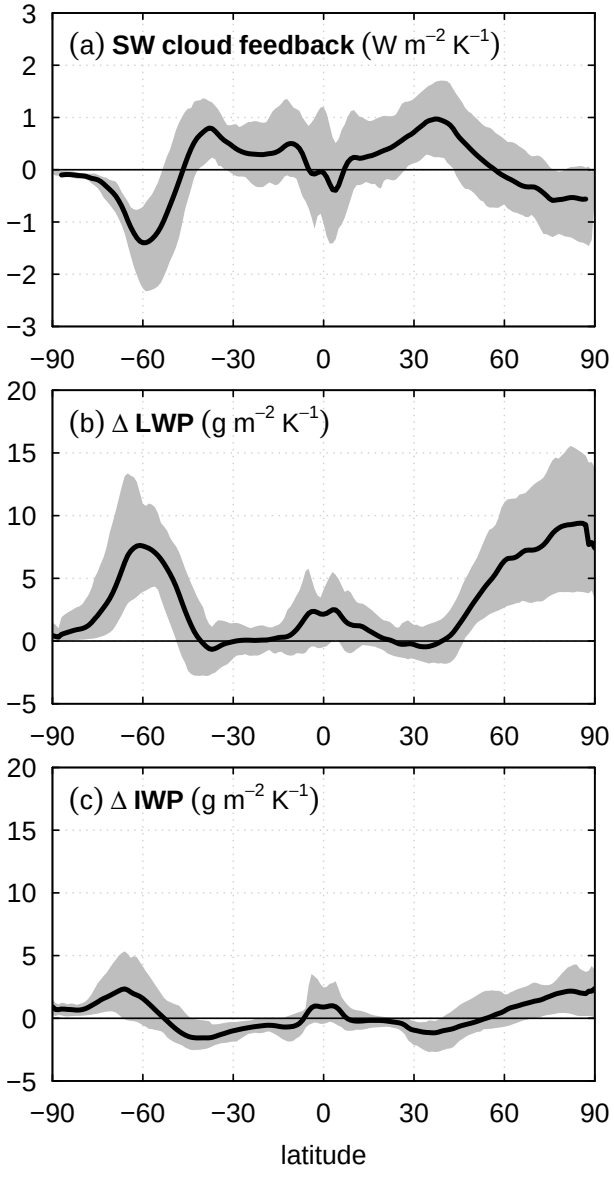

723 FIG. 1. Model responses (2050–2099 minus 1950–1999) in the RCP8.5 experiment of CMIP5, based on
724 the first ensemble member of 32 models. (a) SW cloud feedback, (b) change in LWP, and (c) change in IWP.
725 In all panels, the black curves denote the multi-model mean response and the grey shading includes 75% of
726 the models. The changes are normalized by the global-mean surface temperature increase in each model. The
727 cloud feedback is calculated using the approximate partial radiative perturbation (APRP) method of Taylor et al.
728 (2007), and includes rapid adjustments.

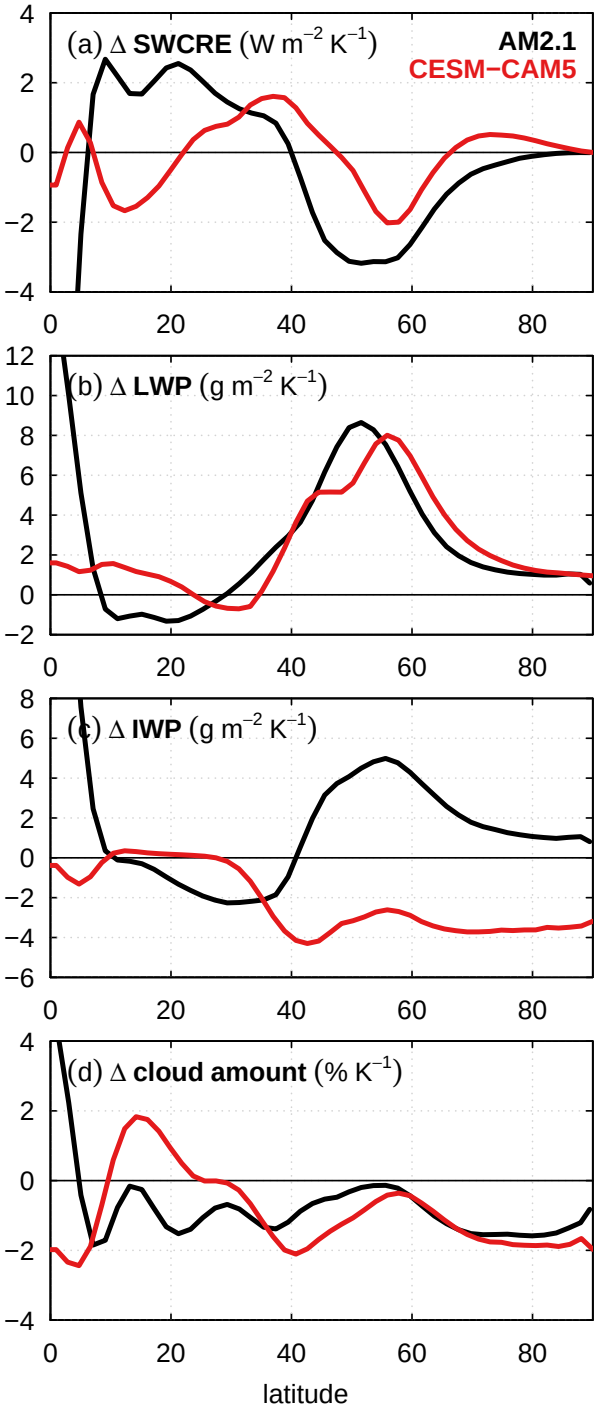

729 FIG. 2. Aquaplanet model responses upon a 4 K SST warming, all normalized by the surface warming: (a)
730 SW cloud radiative effect, (b) LWP, (c) IWP, and (d) cloud fraction. Black and red curves denote AM2.1 and
731 CESM-CAM5, respectively.

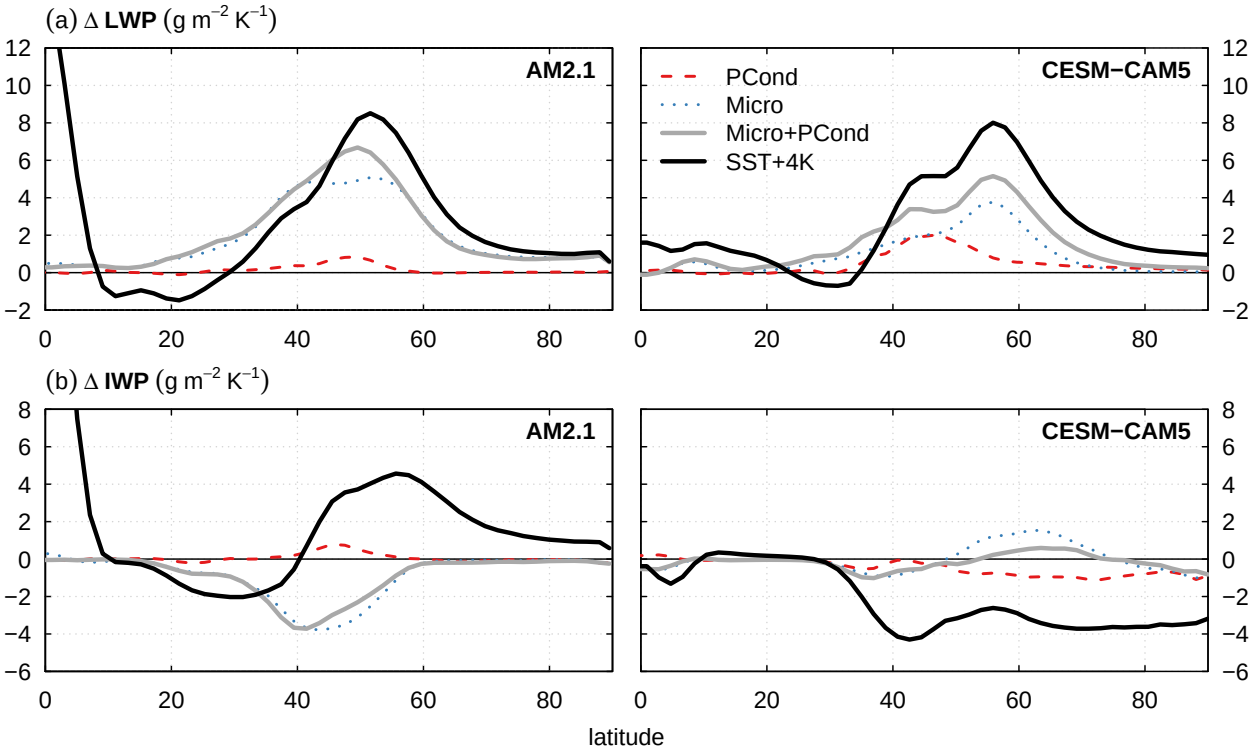

732 FIG. 3. (a) LWP and (b) IWP responses in the PCond (red dashed), Micro (blue dotted), Micro+PCond (thick
733 grey), and SST+4K (thick black) aquaplanet experiments (see Table 1 for a description). All responses are
734 normalized assuming a 4 K warming.

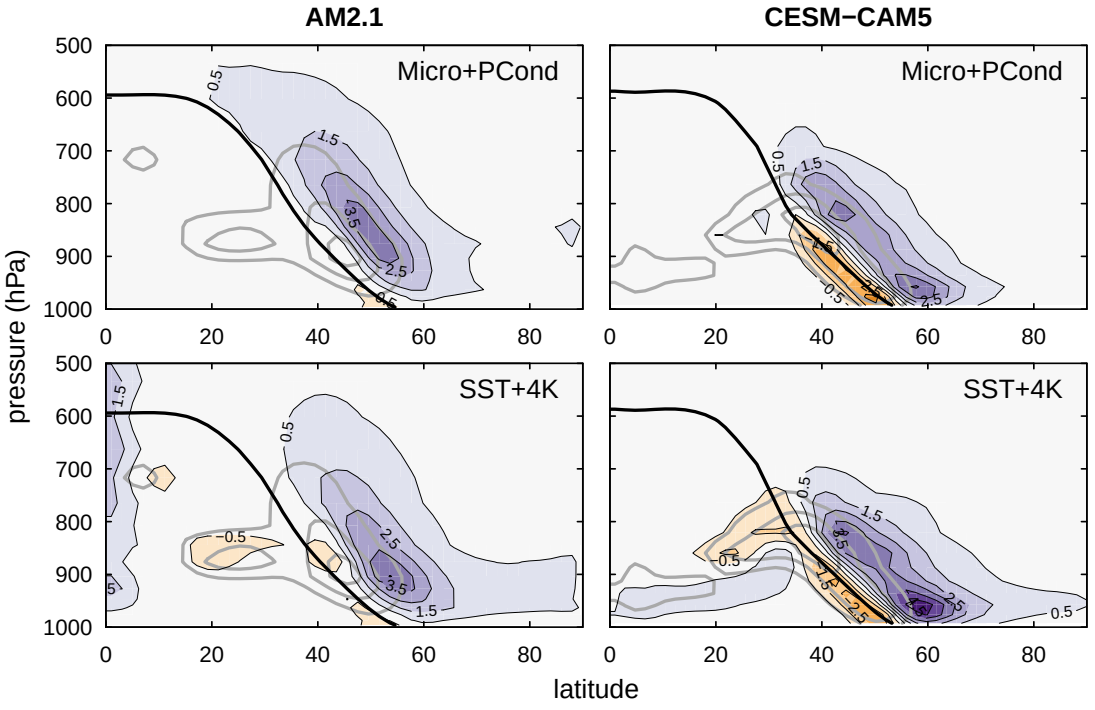

FIG. 4. Changes in cloud liquid water mixing ratio (shading, in mg kg^{-1} K^{-1}) as a function of latitude and pressure in the Micro+PCond and SST+4K aquaplanet experiments. Thick grey contours represent the control climatology (contours every 10 mg kg^{-1}), while the thick black curve denotes the melting line (0°C isotherm).

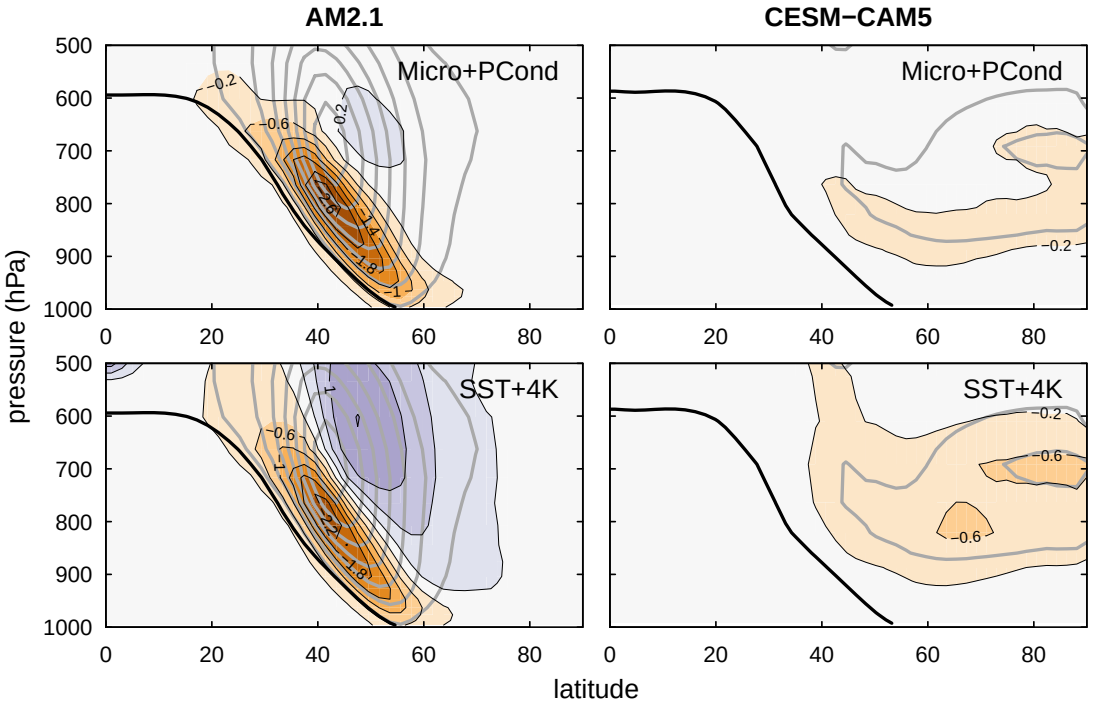

738 FIG. 5. As in Fig. 4, but for changes in cloud ice mixing ratio. The contour interval for the climatology (thick
739 grey contours) is 3 mg kg^{-1}.

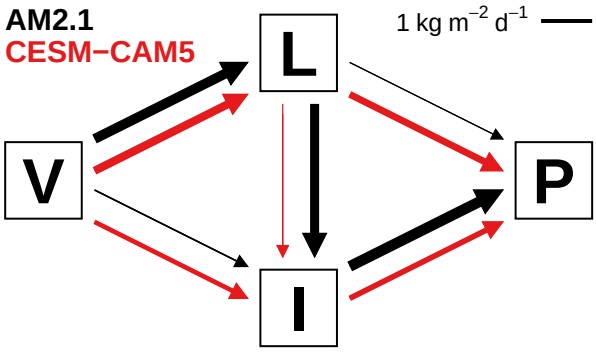

FIG. 6. Net vertically-integrated conversion rates between vapor (V), cloud liquid water (L), cloud ice (I), and precipitation (P) in the aquaplanet control climatology. The conversions from V to L and V to I include contributions from large-scale condensation (in the cloud macrophysics scheme) and detrainment from convection, while all other conversions shown here occur in the cloud microphysics only. The arrow width is proportional to the net conversion rate. Black and red arrows denote AM2.1 and CESM-CAM5, respectively.

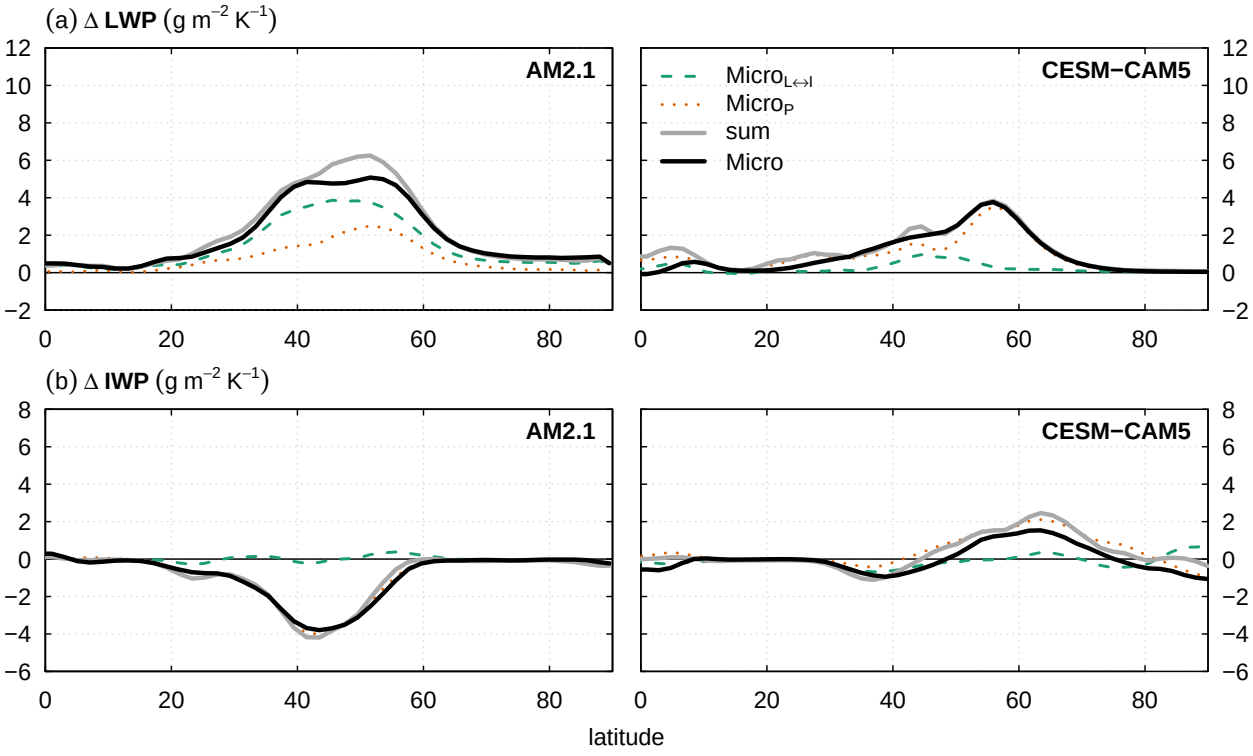

FIG. 7. As in Fig. 3, but showing the LWP and IWP changes in Micro$_{L\leftrightarrow I}$ and Micro$_P$.

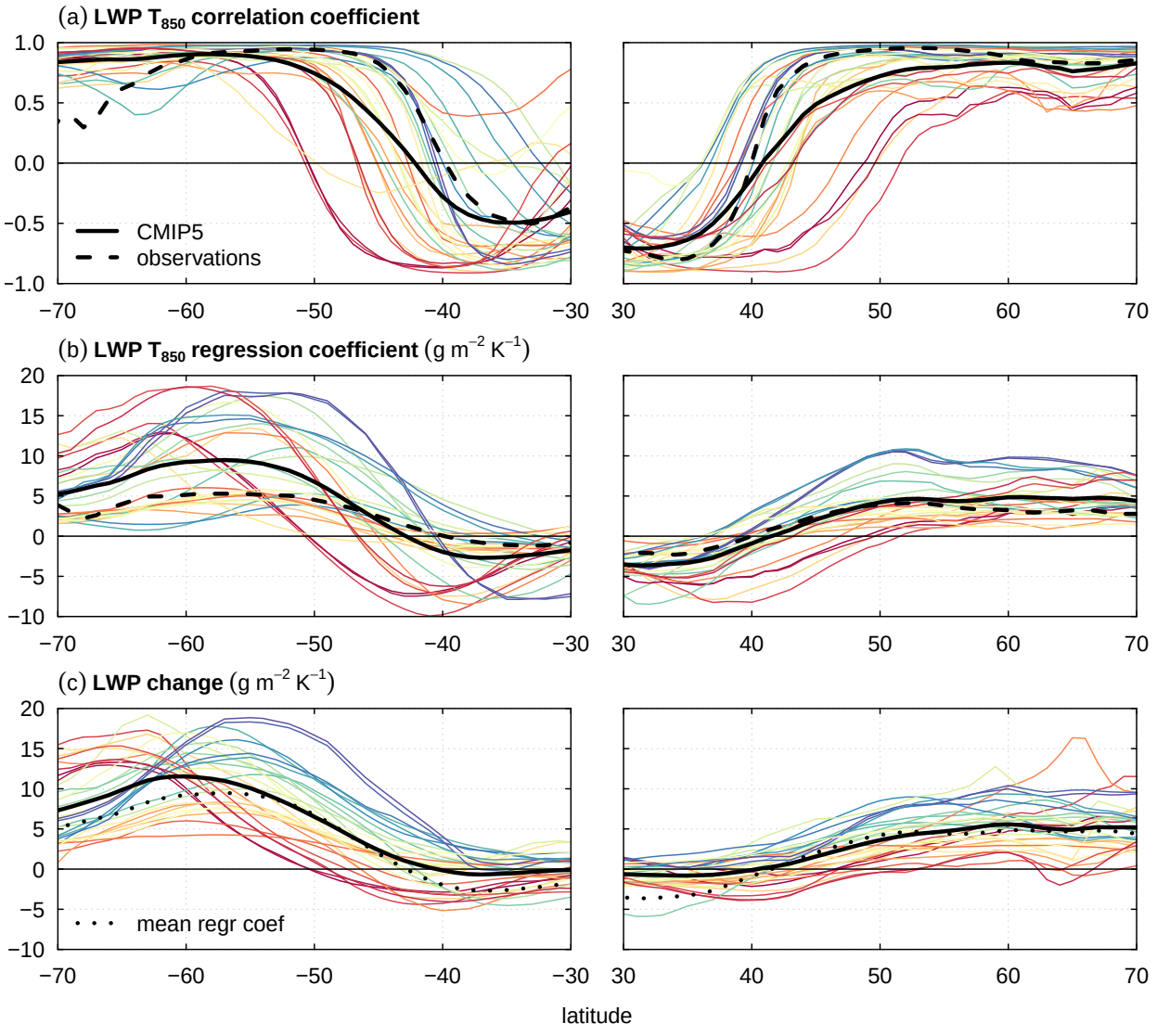

FIG. 8. Relationships between 850 hPa temperature (T_{850}) and LWP in CMIP5 models and observations: (a) correlation between monthly-mean, zonal-mean LWP and T_{850} in the historical experiment of CMIP5 and observations, (b) same but for the regression coefficient of LWP onto T_{850}, and (c) RCP8.5 minus historical LWP response normalized by the local warming in each model. In all panels, colored curves represent individual CMIP5 models with the multi-model mean in thick black, and the dashed black curve denotes observations. The model curves are colored according to the LWP change at 50°S from panel (c). For CMIP5 models, the historical and RCP8.5 periods are 1980–1999 and 2080–2099, respectively. For the observations, LWP satellite observations for 1989–2008 (O'Dell et al. 2008) are combined with ERA-Interim reanalysis temperature (Dee et al. 2011). Because LWP satellite observations are available over oceans only, all land grid points are excluded from the analysis for both models and observations.